STABILITY OF CRACK TIP IN TERMS OF MOLECULAR DYNAMICS

ANNA MACHOVÁ, GLENN E. BELTZ

The conditions for dislocation emission from a crack tip, as well as crack propagation under mode I, are analyzed for bcc iron both with the Rice model based on the Peierls-Nabarro framework and a molecular dynamic technique including virial stresses. The atomistic results with a pair potential agree satisfactorily with the continuum prediction on load conditions for dislocation emission. Crack extension in atomistic simulations is observed when normal virial stress at the crack tip exceeds cohesive strength of the potential.

1. Introduction

Brittle versus ductile behaviour at a crack tip has been intensively studied both within the framework of the Peierls-Nabarro concept in continuum models, such as the model promoted by Rice [1, 2, 3], as well as with atomistic simulations [4–7]. Several recent atomistic studies [4, 6] indicate that load conditions for dislocation emission disagree with the load predicted by Rice's continuum model [1].

The present study is motivated by an effort to understand the discrepancies between atomistic results and continuum models and to contribute to an improvement of the continuum modeling.

Unlike the previous atomistic studies [4, 6], we use molecular dynamic (MD) simulations in conjunction with a different pair potential, one with angular (Y) correction [5], as well as a different boundary condition. Under quasistatic loading, dislocation emission on the $\langle 111 \rangle \{112\}$ slip system intersecting the crack front was observed in [5, 7]. To analyze the stress state at the crack tip during dislocation emission and crack extension, virial stresses [6, 8] were calculated here at specific atoms. Virial stresses correctly describe the nonlinear crack tip zone and enable us to study also the kinetics of crack tip processes. The MD results are compared with the results obtained from the Peierls framework developed by Rice [1].

Ing. A. Machová, CSc., Institute of Thermomechanics AS CR, Dolejškova 5, 18200 Prague 8, CR.

Dr. G. E. Beltz, Dept. of Mech. & Environmental Engineering UCSB Santa Barbara CA 93106-5070, USA.

2. MD simulations

We consider either a perfect crystal of bcc iron oriented so that $x_1 = [-110]$, $x_2 = [001]$, $x_3 = [110]$ under plane strain conditions ($\varepsilon_{33} = \varepsilon_{32} = \varepsilon_{31} = 0$), or the same crystal containing an embedded central, through, pre-existing crack. The bcc lattice is projected to the (110) plane. The projected atoms (Figs. 1 and 3) represent lines of atoms perpendicular to this plane that move simultaneously with the projected atoms. Atomic movement in the perpendicular x_3 direction is not permitted.

In crack simulations, the initial half crack length is $l_0 = 20d_{110}$, and the initial crack opening $c_0 = 1d_{001}$, where $d_{110} = a_0/\sqrt{2}$ and $d_{001} = a_0/2$ denote the interplanar distances in the directions $\langle 110 \rangle$ and $\langle 001 \rangle$, and a_0 denotes the lattice parameter. The crack front is oriented in the x_3 direction, the crack plane is normal to x_2 and the direction of crack extension is x_1. Due to the symmetry, we treat explicitly only one half (Fig. 3) of the rectangular sample containing the central crack. The atoms lying on the symmetry axis x_2 (left border of the simulation box) are constrained against motion in the x_1-direction, and all other atoms are free to move in the x_1 and x_2 directions. The simulation box consists of 50 atomic planes along x_1, 100 along x_2 and 3 along x_3. For the short ranged Y-potential, this small thickness is sufficient to include the entire range of interatomic interactions in the bcc lattice under plain strain conditions. Atomic interactions across the initial crack plane do not exist (it is a pre-existing, traction-free crack). Prior to loading, the atomic sample is relaxed using viscous damping in the Newtonian equations of motion to suppress the influence of surface relaxation on the kinetics of crack tip processes. After this relaxation, the initial crack is loaded quasistatically in mode I by applying external forces in the $\pm x_2$ directions at the sample borders, reaching a prescribed level σ_A during 1000 time integration steps; thereafter, the applied stress is held constant. The Newtonian equations of motion are solved by a central difference method using the time integration step $\Delta t = 1 \times 10^{-14}$ s. The key parameter in the crack simulations is the cutoff radius r_c of the potential: if the distance r between atoms is greater or equal to r_c, the bond is broken; otherwise, the bond exists. We record for each time step the global energy balance and also the existing interatomic bonds near the crack tip, so we can detect each crack advance. Thermal atomic motion is not controlled, i.e. atomic velocities are not prescribed during the simulations.

In order to obtain a Peierls shear stress versus displacement curve, the key material input for continuum models, we considered block like shear on the $\langle 111 \rangle \{112\}$ slip system. For this, we used a rectangular sample with 98 planes along the x_1 direction, 100 planes along x_2, and 3 along x_3. The crystal was divided along a $\{112\}$ plane into two parts: upper part was fixed and the lower part was gradually

Fig. 1. Scheme for block like shear.

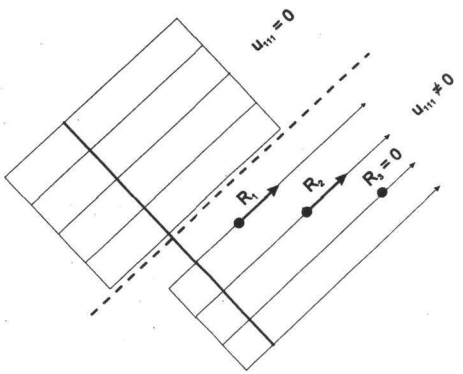

displaced (Fig. 1) in the $\langle 111 \rangle$ direction from $u_{111} = 0$ to $u_{111} = 1b$ using a step $0.01b$, where $b = a_0\sqrt{3/2}$ is the Burgers vector in bcc iron. During the procedure, the MD program evaluated changes in the total potential energy and the resulting forces acting at individual atoms in the $\langle 111 \rangle$ direction, without relaxation of the atoms.

3. Results and discussion

Tab. 1 includes the relevant parameters for the Y-potential and our crystal orientation, which play an important role in atomistic simulations: surface formation energy γ_{001}, anisotropic stiffness C, Griffith stress intensity K_G ($2\gamma_{001} = CK_G^2$), effective Young modulus E and Poisson ratio ν, shear modulus μ in the slip system $\langle 111 \rangle \{112\}$, the cutoff radius r_c, the cohesive strength $\sigma_c(\mathrm{I})$ of the potential and the barrier $\sigma_c(\mathrm{II})$ against breaking of the bonds between the second neighbours (II) in the bcc lattice under axial straining in the $\langle 001 \rangle$ direction.

Table 1. Parameters relevant for present MD simulations, the lattice parameter $a_0 = 2.8660$ Å

r_c/a_0	$\sigma_c(\mathrm{II})/E$	$\sigma_c(\mathrm{I})/E$	ν	E 10^{+11} N/m^2	μ	C 10^{-11} m^2/N	γ_{001} J/m^2	K_G MPa m$^{1/2}$
1.30	0.252	0.363	0.635	1.480	0.718	0.489	1.97	0.90

3.1 Block-like shear and the Peierls prediction for dislocation nucleation

Motivated by the Xu-Argon-Ortiz (XAO) analytical representation [3] of shear stress versus atomic shear displacement ($\tau = (\mu b/2\pi 2h) f(2\pi\Delta/b)$, where the function f is too cumbersome to be presented here), we may make following associations for $\langle 111\rangle\{112\}$ slip: $\Delta/b = u_{111}/b$, $h = a_0/\sqrt{6}$ is the interplanar distance between the $\{112\}$ slip planes, $b = a_0\langle 111\rangle/2$ is Burgers vector and u_{111} is the relative displacement of the two blocks in the $\langle 111\rangle$-slip direction (Fig. 1). The XAO representation permits independent specification of the unstable stacking fault energy and the peak stress τ_c, unlike the Frenkel approximation which uses a sinusoid for $f(2\pi\Delta/b)$. We introduce dimensionless shear stress for presentation of the results according to the relation: $\tau^* = \tau \cdot \text{const}$, where const $= (2\pi^2 h/\mu b) = 1.296 \times 10^{-10}$ Pa^{-1}.

As to atomistic results, we have verified that the unstable stacking fault energy γ_{us} and the critical shear stress τ_c can be determined from the work W_{111} done along the slip plane during block like shear in the $\langle 111\rangle$ direction. For the short ranged Y-potential, non-zero interplanar interactions exist only between the first and the second nearest neighbouring (112) planes. Thus, non-zero resulting forces at individual atoms appear only in the first (R_1) and in the second (R_2) (112) plane of the lower moving part of the crystal in Fig. 1. If one imposes block like shear gradually by steps $u_n = u_{n-1} + \mathrm{d}u$, where $\mathrm{d}u = \mathrm{d}u_{111} = 0.01b$ and $n = 1, 100$, then the work done along the slip plane and the shear stress are given by the relations:

$$W_{111} = \sum_n (R_1+R_2)\mathrm{d}u_{111},\ \tau = \mathrm{d}W_{111}/\mathrm{d}u_{111}/A_{112} = (R_1+R_2)/A_{112},\ \tau^* = \tau\cdot\text{const},$$

where $A_{112} = b \cdot 2d_{110}$ is the area per one atom in a (112) plane. The normalized work W_{111}/A_{112} at the position $u_{111}/b = 0.5$ corresponds to $\gamma_{us} = 0.75$ J/m^2, the maximum critical shear stress is $\tau_c^* = 1.8$ for the Y-potential.

Fig. 2 shows the dimensionless shear stress τ^* as a function of the relative atomic displacement u_{111}/b, as calculated atomistically, as well as the analytical approximation of the atomistic results by the XAO curve [3] using a dimensionless parameter $(2\pi^2 h\gamma_{us}/\mu b^2) = 0.39$. Using a slip plane inclination angle 35° and integral equation methods outlined in [2], the Rice/Peierls model gives a critical energy release rate (G_{Id}) for dislocation nucleation of $12.86\gamma_{us}$. Tab. 2 summarizes the results for dislocation nucleation with the Rice/Peierls model. It includes also the predicted critical stress intensity $K_{IE}/K_G = (G_{Id}/2\gamma_{001})^{1/2}$ needed for emission of an edge dislocation from the crack tip in the slip system $\langle 111\rangle\{112\}$, when crack plane is (001).

The Y-potential leads to oscillations near the position $u_{111}/b = 0.5$ in Fig. 2 because the total potential energy and the W_{111} have a local flat minimum at this

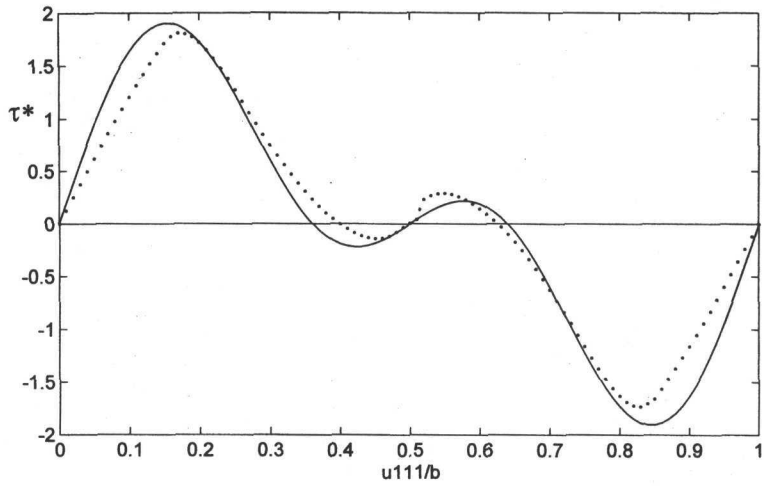

Fig. 2. Shear stress during block like shear for the Y-potential (denoted by dots) and its XAO analytical approximation (denoted by line).

Table 2. Unstable stacking fault energy and critical shear stress as calculated by rigid block sliding and by XAO fit, as well as the energy release rate and the stress intensity factor for dislocation nucleation as predicted by the Peierls/Rice continuum model

Model	γ_{us}/γ_{001}	τ_c^*	G_{Id}/γ_{us}	K_{IE}/K_G
Peierls/Rice	0.38	1.9	12.86	1.56

position during the rigid sliding. It indicates that a dislocation at $b/2$ may exist in a weak metastable position. This does not influence stability of dislocations from the thermodynamical point of view since γ_{us} is relatively high.

3.2 Dislocation emission in the MD simulations

The present results were obtained under the quasistatic loading from 0 up to the Griffith level σ_G. This level corresponds to an applied stress intensity $K_A = F_I\sigma_G(\pi l_0)^{1/2} = 1.4K_G$ due to stress intensification ($F_I = 1.4$ according to [9]) in our finite samples.

Dislocations were generated as early as the linearly increasing phase of loading at the time step NSTEP = 880 (see Fig. 3, where edge dislocation in a slip system $\langle 111\rangle\{112\}$ can be seen at a position $2b$ from the free crack face). The emission is

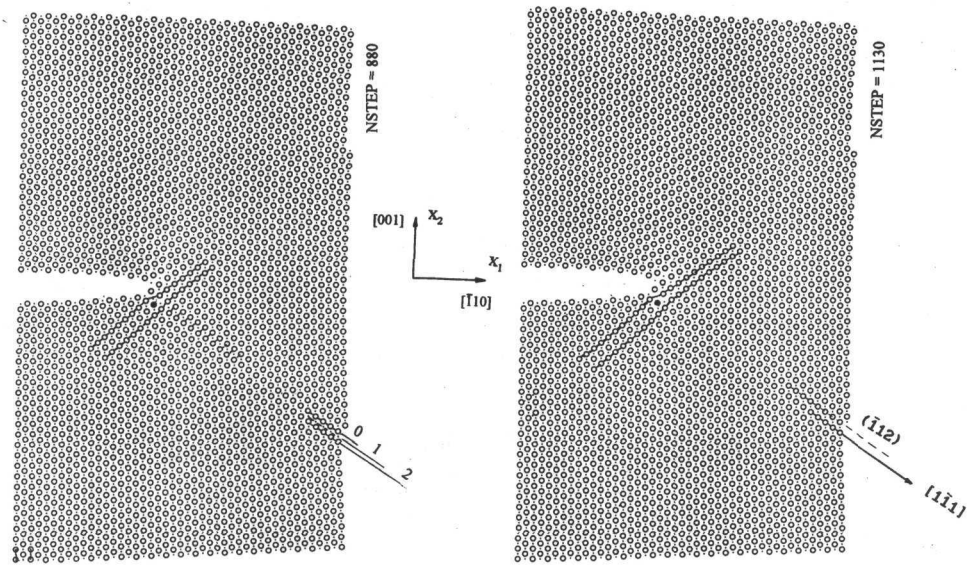

Fig. 3. Dislocation generation in MD simulation – detail at the crack tip. Black circle denotes a leading atom of the dislocation.

accompanied by bond breakage in the slip system. The configuration at NSTEP = 880 is not influenced by the stress waves emitted during the bond breakage and reflected back from external sample borders. The first interatomic bond II was broken at NSTEP = 691. The velocity of longitudinal waves in the direction of the shortest distance to external borders is $C_{L\langle 110\rangle} = 6175$ m/s. The reversal time for back reflections corresponds to 202 time steps, i.e. the crack tip configuration can be influenced at the time step NSTEP = 691 + 202 = 893. The dislocation remains in the same position $r = 2b$ even at NSTEP = 1130 (Fig. 3), when atoms in front of the crack tip experience the full loading $K_A = 1.4K_G$.

It is clear that the critical loading $K_A = 1.4K_G$ needed for dislocation emission in MD simulations lies below the level $K_{IE} = 1.56K_G$ following from the Peierls/Rice model (Tab. 2), which represents a deviation about 10%.

The relative displacements u_{20}, u_{10}, u_{21} of the planes 0, 1, 2 (Fig. 3) during dislocation formation at the crack tip are shown in Fig. 4. It can be seen that the u_{20} reaches at NSTEP = 880 a value about $b/2 = 1.24$ Å, which corresponds to the unstable position during idealized block like shear. The relative displacements differ slightly from the values $u_{10} = u_{20}$, $u_{21} = 0$ for block like shear. It indicates that, beside the influence of the normal relaxation between the slip planes discussed in [2], also different distribution of the shear displacements at the crack tip may

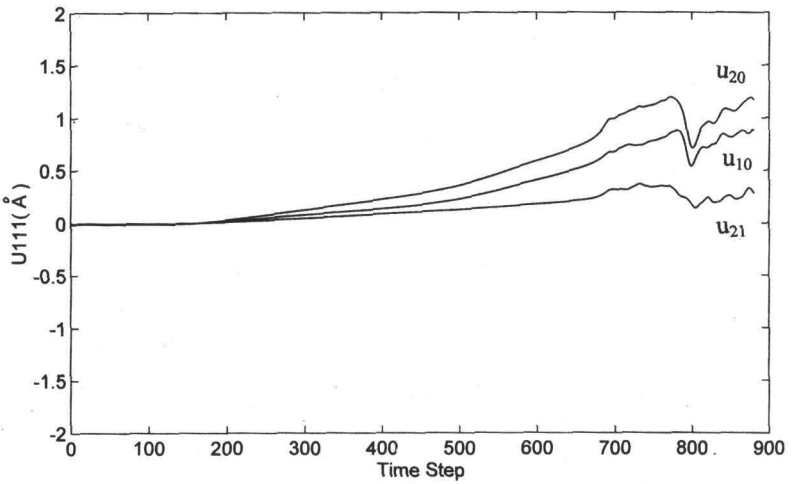

Fig. 4. Relative displacements at the crack tip during dislocation formation in MD simulation.

explain the discrepancies between the Rice model and atomistic results.

Time development of the shear virial stress at one leading atom of the dislocation (denoted in Fig. 3 by the full circle) is shown in Fig. 5. Part (a) represents the nonlinear contribution arising from the potential energy, and part (b) is the contribution arising from the kinetic energy at the crack tip. The latter illustrates that the loading is quasistatic up to NSTEP = 691, when the first bond II between the second neighbours has been broken at the crack tip in the slip system. After that, the leading atom oscillates in the ⟨111⟩ directions during the dislocation formation, similar to thermal activation. Nevertheless, the kinetic contribution is very small in comparison with the virial shear stress (a) from the potential energy. Fig. 5a shows that the dislocation is generated when the maximum virial shear stress overcomes the critical value τ_c^* following from the Peierls/Rice model (Tab. 2). It is also valid for the other interior atoms lying in the slip plane No. 2 in Fig. 3, when the dislocation moves into the crystal.

Time development of the normal virial stress at the crack tip shows that the bond II in the slip system is broken and the dislocation is generated when the normal virial stress reaches a maximum where it exceeds the barrier σ_c(II) from Tab. 1. Later, at NSTEP = 789, the bond II is reformed and at NSTEP = 835, it is broken again (refer to the transient oscillations in Figs. 4 and 5). The present results and the results in [7] indicate that the barrier σ_c (II) in the theoretical tension diagram plays a role of the "yield" stress for the short ranged potentials.

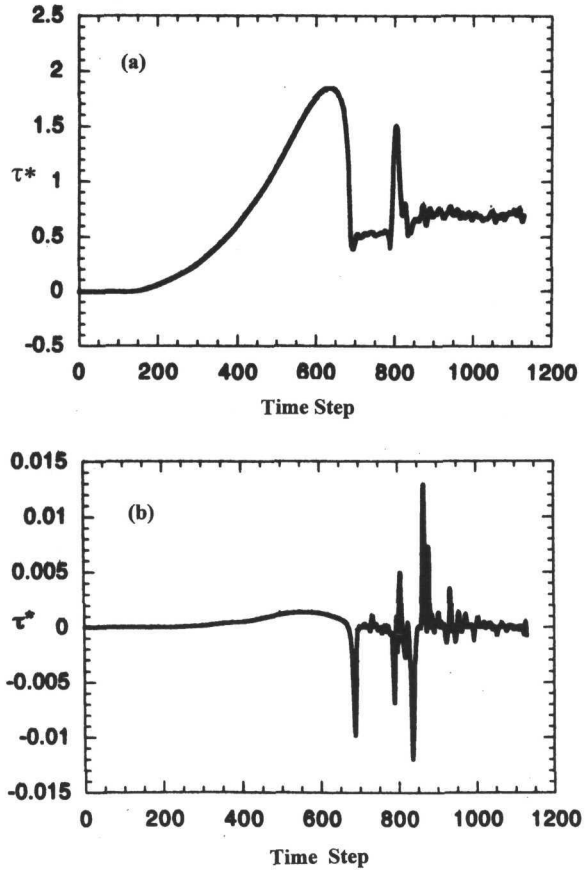

Fig. 5. Shear virial stress near the crack tip during dislocation formation in MD simulation: (a) – contribution from the potential energy, (b) – contribution from the kinetic energy.

Our results concerning the distribution of relative slip displacement at the crack tip and the virial stress at interior atoms in the slip plane are consistent with other studies that indicate that the stress versus displacement curve at the crack tip (or near a surface) is somewhat different from its bulk form. However, the shear resistance appears to decrease near free crack faces, which is at odds with prevailing view point that ledge formation near a surface should hinder, not promote, dislocation formation [3]. Figs. 4 and 5 also show that the dislocation in Fig. 3 is kept at the crack tip in the unstable position $u_{20} \sim b/2$ under non-zero shear stress, while according to Peierls/Rice model $\tau^* = 0$ for $u = b/2$, i.e. there is no lattice-resistance and the emitted dislocation is assumed to move far away. These issues will be addressed in future work.

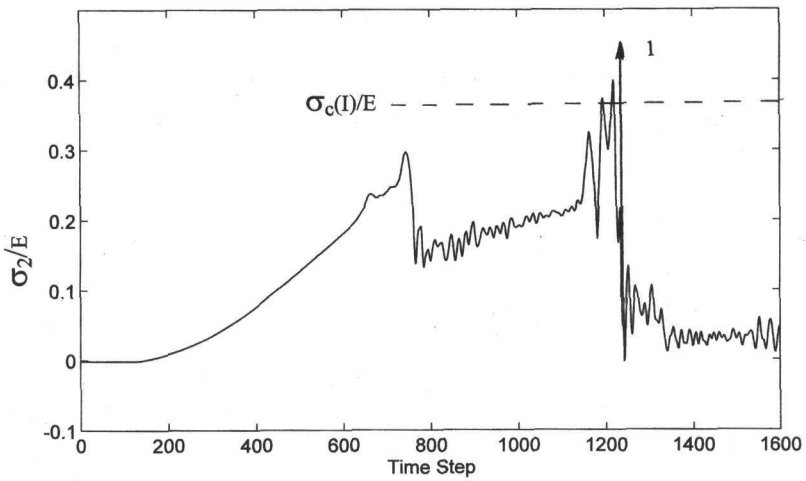

Fig. 6. Normal virial stress in MD simulation of crack extension.

3.3 Crack extension in the MD simulations

The lowest (i.e. critical) loading, when crack extension was monitored in our simulations, corresponds to $\sigma_A = 1.11\sigma_G$, i.e. to $K_A = K_{IC} = 1.554K_G$, which agrees well with the results in [7] using a different loading rate.

Time development of the normal virial stress σ_2/E at crack initiation is illustrated for one crack tip atom in Fig. 6. The figure shows that after the initial increase of the normal stress during the linear loading regime, a decrease of the stress appears at NSTEP = 800 due to the shielding effect of an emitted dislocation (similar to Fig. 3), which precedes crack initiation. Since the applied forces at external borders increase up to NSTEP = 1000, the normal virial stress in Fig. 6 for NSTEP > 800 gradually increases, until it exceeds the ideal cohesive strength $\sigma_c(I)/E$ of the potential denoted by the dashed line. The first elementary crack advance by 1 d_{110} is denoted in Fig. 6 by the arrow 1, which appears at NSTEP = =1236. It causes the normal virial stress to decrease to zero since for NSTEP > 1236 the atom under consideration lies on a free crack face after the crack extension.

Crack extension is already influenced by reflections of the stress waves from external sample borders mentioned above. During the crack extension we have calculated each time step the normal virial stresses at 10 atoms lying at the axis of crack propagation. The results are similar to those shown in Fig. 6, and they show that in each case, to realize a continued crack advance, the normal virial stress at the moving crack tip needs to overcome the cohesive strength $\sigma_c(I)$ of the potential. This supports the cohesive zone model of failure.

4. Conclusions

1. The critical loading $K_{IE} = 1.4K_G$ needed for dislocation emission from the crack tip in MD simulations lies for the Y potential [5] about 10% below the level predicted by the (shear-only) Rice model, which is in turn based on the Peierls--Nabarro concept.

2. Calculations of the shear stress in framework of the Peierls-Nabarro (block like shear) model and of the virial shear stresses in MD simulations show that interior atoms, lying on the dislocation slip plane, need to overcome the critical shear stress from Peierls-Nabarro model during dislocation emission in MD simulations.

3. Emission of shielding dislocations precedes the initiation of crack propagation in present MD simulations. Crack extension is monitored when the normal virial stress at the crack front exceeds the ideal strength of the potential which supports the cohesive model of failure. The critical loading needed for crack extension in MD simulations corresponds to $K_{IC} = 1.554K_G$.

Acknowledgements. The work was supported by a CR-USA grant (KONTAKT 058) and by the Grant Agency AS CR in Prague under contract A2076701, as well as the National Science Foundation (USA) under grant INT-9707863.

REFERENCES

[1] RICE, J. R.: J. Mech. Phys. Solids, *40,* 1992, p. 239.
[2] SUN, Y.—BELTZ, G. E.—RICE, J. R.: Mater. Sci. Eng., *A170,* 1993, p. 67.
[3] XU, G.—ARGON, A. S.—ORTIZ, M.: Phil. Mag., *A72,* 1995, p. 415.
[4] SHASTRY, V.—FARKAS, D.: Modelling Simul. Mater. Sci. Eng., *4,* 1996, p. 161.
[5] MACHOVÁ, A.: Mater. Sci. Eng., *A206,* 1996, p. 279; Mater. Sci. Eng., *A149,* 1992, p. 153.
[6] CLERI, F.—YIP, S.—WOLF, D.—PHILLPOT, S. R.: Phys. Rev. Letters, *79/7,* 1997, p. 1309.
[7] MACHOVÁ, A.—KROUPA, F.: Mater. Sci. Eng., *A234–236,* 1997, p. 185.
[8] LUTSKO, J. F.: In: Computer Simulations in Materials Science. Eds.: Meyer, M., Pontikis, V. Kluwer 1991, NATO ASI Series, p. 341.
[9] MURAKAMI, Y.: (Ed.), Stress Intensity Factor Handbook. Vol. 1, Oxford, Pergamon 1987, p. 67.
[10] LIN, L. H.—THOMSON, R.: Acta Metall., *34,* 1986, p. 187.